Scripta Materialia 247 (2024) 116097

Contents lists available at ScienceDirect

Scripta Materialia

journal homepage: www.journals.elsevier.com/scripta-materialia

Vortex-like magnetic domain evolution in soft magnetic dual-phase Fe-Co-Ti-Ge compositionally complex alloy

Xukai Zhang *, Gerhard Dehm, Christian H. Liebscher *

Max-Planck-Institut für Eisenforschung GmbH, Max-Planck-Straße 1, 40237, Düsseldorf, Germany

ARTICLE INFO

Keywords:
Fe-Co-Ti-Ge alloy
Soft magnetic material
Magnetic domain
Lorentz TEM
Differential phase contrast STEM

ABSTRACT

Soft magnetic compositionally complex alloys (CCAs) have attracted great attention in recent years. However, the magnetic domain structures and magnetic properties have rarely been studied in a correlative way for dual-phase CCAs. Here we investigate the microstructure and magnetic domain structure of a recently proposed dual-phase $Fe_{30}Co_{40}Ti_{10}Ge_{20}$ CCA using scanning transmission electron microscopy-energy dispersive spectroscopy (STEM-EDS), Lorentz TEM, differential phase contrast (DPC)-STEM and 4D-STEM. Three types of Fe-Co-rich phases with different shapes were discerned in the Heusler phase matrix. The magnetic domain type of the Fe-Co-rich phase is determined by its shape. A new vortex-like structure with subdomains in the Fe-Co-rich phase was observed. The evolution of magnetic domain structure was investigated by *in situ* Lorentz TEM experiments and correlated to the microstructure. These results provide insights into understanding the magnetic domain structure in Fe-Co-Ni-based magnetic CCAs to design CCAs with better magnetic performance by manipulating the microstructure.

There has been a growing interest in the magnetic properties of compositionally complex alloys (CCAs), especially those alloyed with Fe, Co and Ni [1–6], except for their excellent mechanical properties as potential structural material applications. Similar to high entropy alloys (HEAs), CCAs contain multiple elements in high concentration [7,8], but consist of multiple ordered or disordered phases enabling to tune their magnetic properties by composition and phase arrangement [5,9]. Although bulk magnetic properties and microstructure evolution have been reported for magnetic CCAs/HEAs, magnetic domain structures and their impact on magnetic properties are rarely studied. It is of significant importance to correlate the microstructure and magnetic domain structure to understand and advance the magnetic behavior. Recently, Lan et al. investigated the magnetic microstructure of the disordered A2 phase and ordered B2 phase in AlCo(Cr)FeNi alloys using off-axis electron holography and Lorentz TEM [10]. They found that a magnetic vortex structure evolves in nanoscale disordered A2 precipitate embedded in an ordered B2 matrix. Radlinger et al. studied the magnetic domain structure and the evolution of spinodally decomposed $Cu_{52}Ni_{34}Fe_{14}$ alloys using STEM-related techniques and magnetic force microscopy (MFM) [11]. Mechanisms related to the magnetic domain structure contributing to coercivity were revealed by Zhou et al. using Lorentz TEM in alnico alloys [9], whereas Kovács et al. showed a coupling between the multi-phase structure and motion of magnetic domain walls using *in situ* Lorentz TEM in an $Al_{0.3}$CoFeNi CCA [12].

In our recent paper [13], we designed dual-phase Fe-Co-Ti-Ge CCAs by introducing a ferromagnetic Fe-Co-Ti-Ge-based $L2_1$-ordered Heusler phase and a Fe-Co-rich BCC-A2 phase, which showed a good combination of high Curie temperature, moderate saturation magnetization and coercivity. Here we investigate both the microstructure and magnetic domain structure evolution of a proposed dual-phase $Fe_{30}Co_{40}Ti_{10}Ge_{20}$ CCA using S/TEM-related techniques and correlate the magnetic domain structure with the emerging microstructure. We show that the magnetic domain structure of the Fe-Co-rich phase is shape-determined. Moreover, we observe a new vortex-like structure with subdomains in the Fe-Co-rich A2 phases and their strong interaction with magnetic domains of the surrounding Heusler phase. These results provide a fundamental understanding of the magnetic domain structure evolution in soft-magnetic CCAs laying the foundation to design CCAs with tailorable magnetic performance by manipulating their microstructure.

An alloy with nominal composition given in atomic percent throughout the paper of $Fe_{30}Co_{40}Ti_{10}Ge_{20}$ (at.%) was investigated in its as-cast state. The production of the investigated alloy has been described elsewhere [13]. The microstructure was investigated in STEM. A plan-view focused ion beam (FIB) lamella was lifted out along [011]

* Corresponding authors.
E-mail addresses: x.zhang@mpie.de (X. Zhang), liebscher@mpie.de (C.H. Liebscher).

https://doi.org/10.1016/j.scriptamat.2024.116097
Received 18 January 2024; Received in revised form 14 March 2024; Accepted 23 March 2024
Available online 8 April 2024

crystal direction using a Scios2HiVac dual beam microscope based on electron back scattered diffraction (EBSD) investigations. STEM observations of the FIB lamella were performed at an acceleration voltage of 300 kV with a probe-corrected Titan Themis 60–300, which is equipped with four synchronized EDS detectors (ChemiSTEM system). Magnetic domains were imaged with Lorentz TEM and DPC-STEM. Lorentz TEM investigations were performed with an image-corrected Titan Themis G2 microscope at 300 kV. In and out-of-focus Lorentz images were obtained in Fresnel mode at a magnetic-field-free atmosphere by completely turning off the objective lens. Further, *in situ* Lorentz experiments were conducted within the magnetic field range of −214 to 315 kA/m by varying the objective lens strength. The magnetic field data at the specimen was provided by the Ernst Ruska Center for the same super twin pole piece configuration determined using a Hall-probe TEM holder. The external magnetic field was applied almost perpendicular to the FIB lamella. Yet, to minimize the artifacts stemming from sample bending, the TEM specimen was slightly tilted (angle $\alpha < 3^{\circ}$) away from a strong diffraction condition, which was also applied for DPC-STEM imaging. DPC-STEM was performed in a probe-corrected Titan Themis 60–300 at 300 kV with a segmented detector with four quadrants. The images were taken in low-magnification mode in which the objective length strength was set manually to a near-zero value and the semi-convergence angle was 0.24 mrad. It should be mentioned that residual magnetic stray fields are still present in the sample under these low-magnification STEM conditions. However, we image the same sample regions by Lorentz TEM and DPC-STEM to draw conclusions on both magnetic domain walls under zero-field conditions and magnetic domains with DPC-STEM. 4D-STEM measurements were performed in a Spectra 200 (Thermo Fisher Scientific) operated at 200 kV in low magnification STEM conditions to minimize the magnetic field stemming from the objective lens. A probe semi-convergence angle of 0.40 mrad was used and nanobeam diffraction patterns were recorded in each probe position with the DECTRIS ARINA hybrid pixel detector (192 × 192 pixel^2). Each scan grid contained 1024 × 1024 pixel^2 and a pixel dwell time of 40 μs was used. The center-of-mass (COM) images were reconstructed using the open-source software package py4DSTEM. All magnetic induction maps either obtained by DPC-STEM or 4D-STEM were generated using the open-source package EMPyRE [14]. It should be emphasized that compositional variations and dynamical diffraction effects, for example, introduced by local sample bending, can affect the determination of the center of mass shifts and thus impact the DPC and 4D-STEM results.

The microstructure of the as-cast $Fe_{30}Co_{40}Ti_{10}Ge_{20}$ alloy is composed of Fe-Co-Ti-Ge Heusler dendrites and interdendrites in which Fe-Co-rich phase form inside of Fe-Co-Ti-Ge Heusler matrix [13]. A plan-view FIB lamella was lifted out in the interdendritic region to gain deeper insight into the structural and compositional features of the two phases and to correlate them to the magnetic domain structure. Fig. 1a shows a low angle annular dark field (LAADF)-STEM image of the Fe-Co-rich and Fe-Co-Ti-Ge Heusler phases in the interdendritic region, and the corresponding STEM-EDS elemental mapping is shown in Fig. 1b. The composition of the Fe-Co-rich phase and Heusler phase is $Fe_{53}Co_{39}Ti_1Ge_7$ (at.%) and $Fe_{27}Co_{45}Ti_{10}Ge_{18}$ (at.%), respectively. The Fe-Co-rich phase has a disordered A2 structure while the Heusler phase shows an ordered $L2_1$ structure (see Fig. S1 in the Supplementary Material). Three types of Fe-Co-rich phases with different morphologies are discerned: spherical ones with a mean diameter of 0.6 μm; elongated ones with an average cross-section of 0.5 μm × 0.2 μm; and large irregular ones. The co-existence of the spherical and elongated Fe-Co-rich phases rather than a cylindrical phase can be concluded by the higher number density of the spherical ones than the elongated ones (see the overview SEM image in Ref. [13]) and the round shape in two vertical directions (see Fig. S1a in Supplementary Section). In all cases, an interfacial dislocation network is observed between the Fe-Co-rich and Heusler phases, indicating that the interface is semi-coherent.

Fig. 2a shows an in-focus Lorentz image of the three types of Fe-Co-rich phases with different morphologies (marked in white) within the Heusler matrix phase. Out-of-focus Lorentz images are shown in Fig. 2b (defocus −500 μm) and Fig. 2c (defocus 500 μm), in which magnetic domain walls present themselves as alternating bright and dark lines. Fig. 2b and c show that the elongated Fe-Co-rich phases are single magnetic domain structures, whereas the spherical and irregular Fe-Co-rich as well as the Heusler matrix phase develop into a sub-domain structure. Fig. 2d is the corresponding DPC-STEM image of the same specimen region imaged in Fig. 2a-c. The color wheel indicates the direction of the in-plane orientation of the magnetization in each domain. It should be noted that the DPC-STEM image was taken in low-magnification mode in which the objective lens excitation is strongly reduced, but the absolute magnetic field at the sample is not necessarily zero. Thus, minor magnetic stray fields can change the magnetic domain structure, resulting in a slightly different magnetic state as shown in the DPC-STEM image compared to its corresponding Lorentz images (Fig. 2b and c). The in-plane magnetic induction of the spherical Fe-Co-rich phases has a closure flux, either clockwise or anti-clockwise. Here we term this magnetic domain structure as vortex-like structure with sub-domains. This structure can be recognized in out-of-focus Lorentz images: a bright or dark spot, representing an edge-on view of the vortex core, is observed within the particles, with an opposite contrast of the

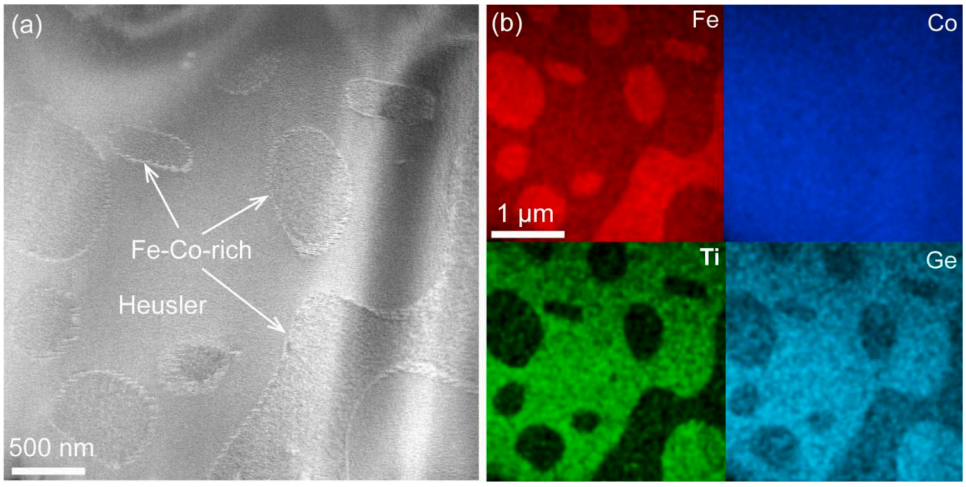

Fig. 1. (a) LAADF-STEM image showing the Fe-Co-rich and Fe-Co-Ti-Ge-type Heusler phases in the interdendritic region in the as-cast $Fe_{30}Co_{40}Ti_{10}Ge_{20}$ (at.%) alloy, (b) STEM-EDS elemental mapping of (a).

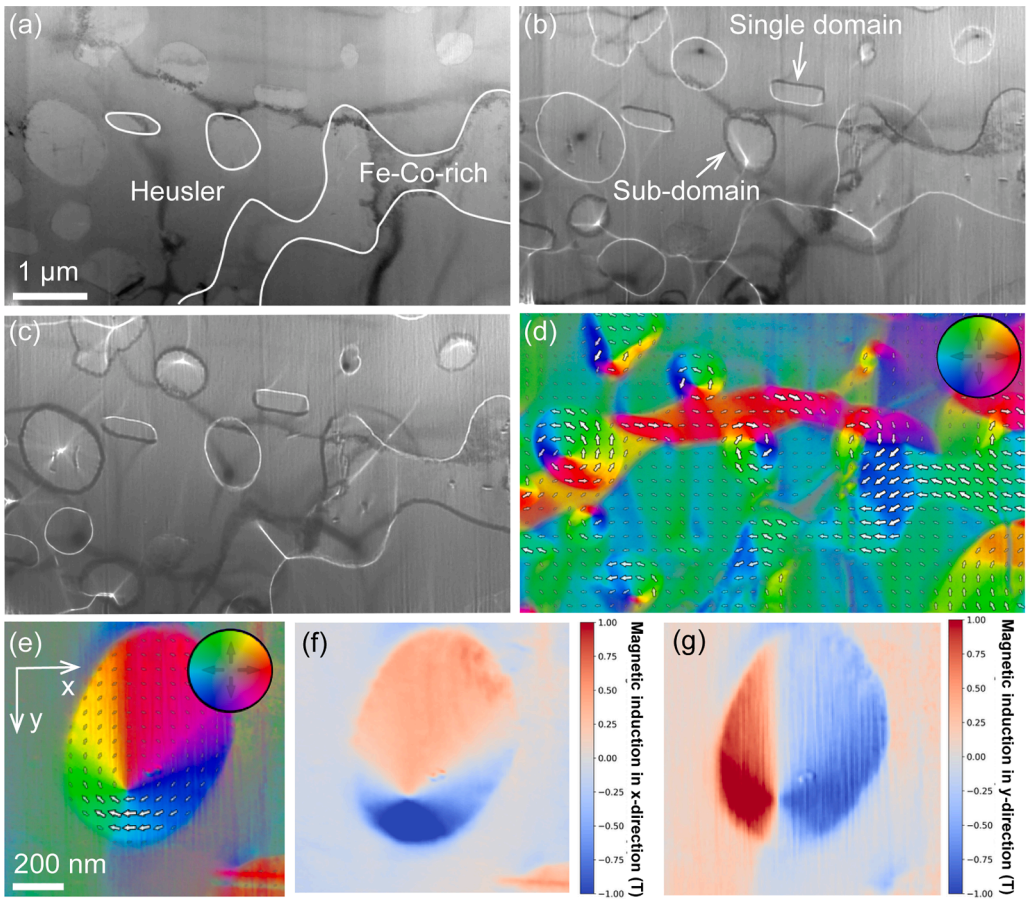

Fig. 2. Lorentz TEM images (a) in focus (the three types of Fe-Co-rich phase with different morphologies are marked in white), with defocus of (b) −500 μm and (c) 500 μm, showing the magnetic domain walls with alternating bright and dark lines, (d) DPC-STEM image with the color wheel inserted at the top right corner and arrows indicating the in-plane induction strength and direction, (e) 4D-STEM image with the color wheel inserted at the top right corner, (f) magnetic induction in the *x*-direction of (e), (g) magnetic induction in the *y*-direction of (e).

domain wall enclosing the precipitate, while several domain walls extend from the core to the interface. Since the vortex structures are observed by Lorentz TEM imaging and low-field DPC-STEM it can be inferred that they are stable against small external magnetic field variations. Fig. 2d indicates that the in-plane magnetic induction of the Fe-Co-rich phase is stronger than that of the Heusler phase and the adjacent Fe-Co-rich and Heusler phases align in a similar direction. To quantify the relative magnetic induction of the two phases, we performed 4D-STEM measurements. Fig. 2e shows a reconstructed DPC map of a spherical Fe-Co-rich phase and its surrounding Heusler matrix phase. The magnetic induction of the phases was obtained using the methods described in [15]. The magnetic induction in the *x* and *y* directions is shown in Fig. 2f and g, respectively, which is roughly 6 times higher for the Fe-Co-rich phase compared to the Heusler phase. We emphasize here that these quantitative measurements depend on the residual magnetic field at the sample, where we study in particular the stability of the vortex structure by *in situ* Lorentz experiments.

Magnetic vortex structure has been extensively studied in 2D thin films [16–18], but remained a theoretical prediction in 3D bulk material [19]. Donnelly et al. used X-ray magnetic nanotomography to reconstruct magnetic vortices through magnetic vorticity within a 3D $GdCo_2$ micropillar and found two types of magnetic vortices: one type is made up of parallel vortex and anti-vortex loops, which are very similar to smoke rings; and in the other type the loops cross over each other, forming singularities [20]. It is unclear whether the magnetic structure of the spherical Fe-Co-rich phases in the bulk sample is the same as those in the FIB lamella since the diameter of the spherical Fe-Co-rich phases (mostly larger than 400 nm) is much larger than the thickness of the FIB lamella (100 - 200 nm). Yet, in another specimen with a thickness of ~ 500 nm, a spherical Fe-Co-rich phase of ~ 400 nm also shows a vortex structure (Fig. S3a), suggesting that they are stable in the bulk. The reconstructed DPC image of the 4D-STEM dataset even shows vortex-like structures for spherical Fe-Co-rich phases with diameters between 50 and 100 nm (Fig. S3b). Currently, there are no techniques available to image nanoscale 3D magnetic microstructures in bulk samples and a combination of several methods (MFM-, TEM- and X-ray based) is needed in combination with micromagnetic simulations [21] to fully explore domain structures in bulk samples.

Fig. 3a shows a DPC-STEM image from another sample, where it becomes apparent that the magnetic domain type of isolated Fe-Co-rich phases seems to be shape-dependent (Fig. 2d, Fig. 3a and Fig. S1b). Plate-like phases with a high aspect ratio adopt a single-domain structure, while spherical ones show vortices. The influence of the phase size and aspect ratio δ (the length of the long axis divided by its short axis) on the magnetic domain type is illustrated in Fig. 3b. The analysis results indicate that isolated Fe-Co-rich phases show a single magnetic domain structure when $\delta > 1.6$ while developing into a vortex-like structure with subdomains when $1 < \delta < 1.6$. This is most likely related to the shape anisotropy of the Fe-Co-rich phases. The crystal orientation of all the Fe-Co-rich phases is confirmed to be the same based on the selected area diffraction result (see Fig. S4). This conclusion agrees with the results observed in Fe particles by Hanson et al. [22] who found that circular particles with a diameter of 550 nm have closed magnetic domain structures with a fourfold symmetry, whereas small circular particles with a diameter of 200 nm and elliptical ones (~450 nm by 150 nm) are considered to be a stable single domain. A single-domain magnetic

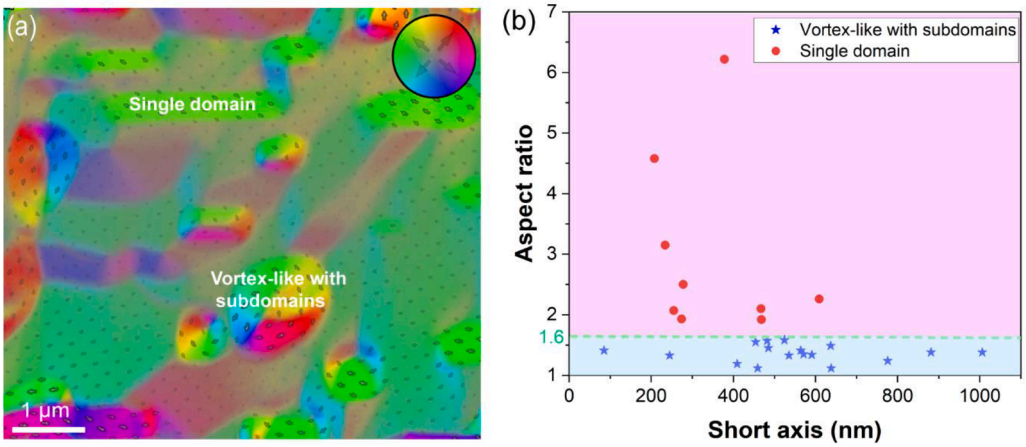

Fig. 3. (a) DPC-STEM image from another FIB lamella (with the color wheel inserted at the top right corner and arrows indicating the in-plane induction strength and direction), (b) the magnetic domain type of the isolated Fe-Co-rich phases is determined by the shape (all Fe-Co-rich phases have the same crystal orientation).

vortex structure in spherical Fe-Cr-rich phases with diameters of 50–120 nm was imaged in a FeCrAlCoNi alloy [10]. Furthermore, Venkateswaran et al. observed magnetic vortex structures in austenitic Ni_2MnGa Heusler alloys and ascribed them to the low magnetocrystalline anisotropy of the austenitic phase [23]. These considerations suggest that besides the size and shape dependence, there is a critical size from developing into a vortex structure with a single domain to one with subdomains.

In situ Lorentz experiments were performed to investigate the dynamics of the magnetic domain walls and the evolution of magnetic

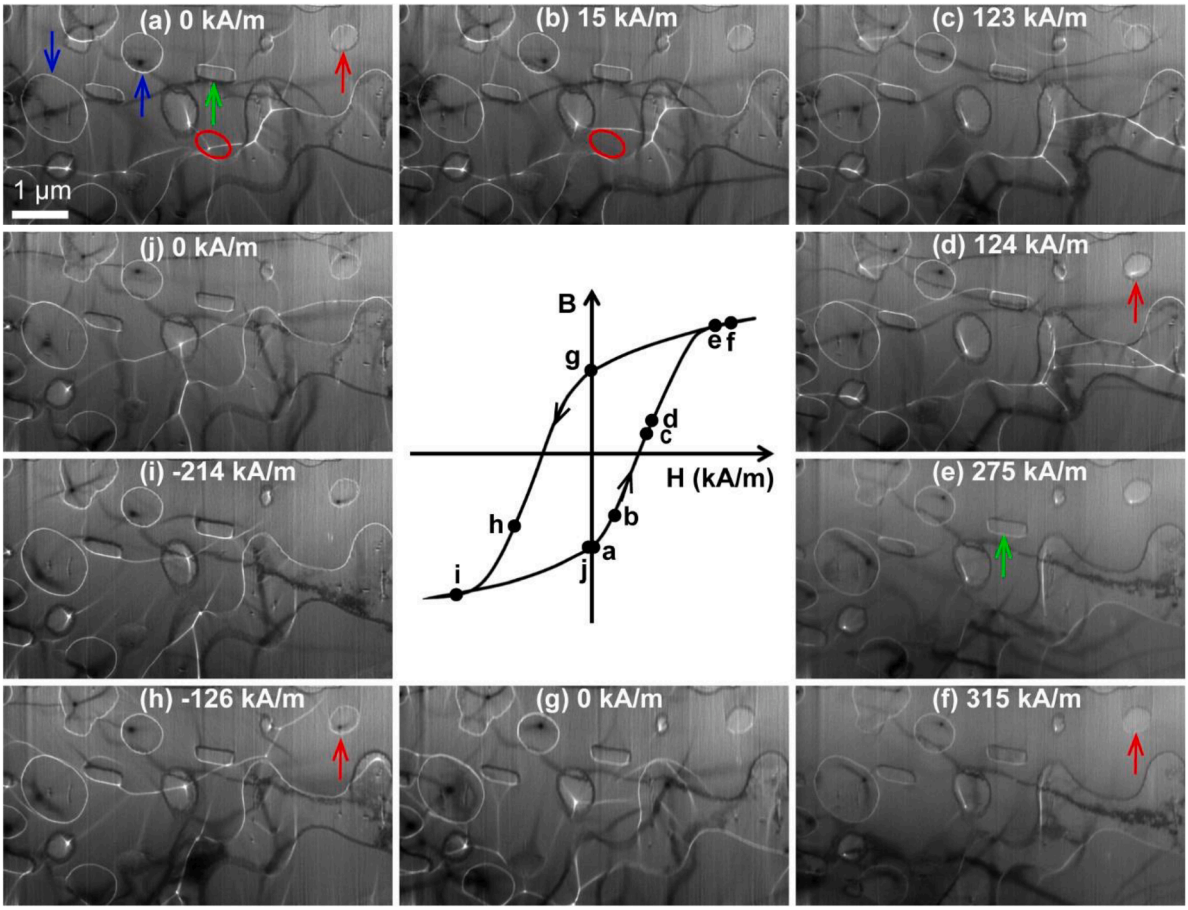

Fig. 4. (a - j) Lorentz TEM images with a defocus of −500 μm at different magnetic fields during *in situ* Lorentz experiments, showing the movement of magnetic domain walls and the evolution of magnetic domains. The hysteresis curve indicates schematically under which magnetic field *H* and magnetization *B* each image was taken. The magnetic domain walls in the Heusler phase first start to move with the increase in the magnetic field (indicated by the red circle in (a) and (b)). The elongated Fe-Co-rich phases with a single magnetic domain remain in their state, but the domain wall contrast changes (indicated by the green arrow in (a) and (e)). Most isolated spherical Fe-Co-rich phases remain in their vortex-like domain state (indicated by the blue arrows in (a)-(j)) except that a magnetic domain structure switch between the single magnetic domain and the vortex-like structure is observed for a small spherical Fe-Co-rich phase (indicated by the red arrow in (a), (d), (f) and (h)).

domains under an externally applied magnetic field. The alloy reaches magnetization saturation when the external magnetic field is ~ ± 150 kA/m [13]. In this experiment, the magnetic field first increased from 0 kA/m to 315 kA/m, followed by a decrease back to 0 kA/m and further down to −214 kA/m, and finally back to 0 kA/m. Lorentz TEM images were taken in Fresnel mode with a defocus of −500 μm. A video showing the dynamic movement of the magnetic domain walls can be found in the supplementary material.

Fig. 4a-j shows ten Lorentz TEM images under different external magnetic fields (illustrated in a schematic *B-H* loop). The magnetic domain walls in the Heusler phase (indicated by the red circle) begin to move first when the magnetic field is increased to 15 kA/m (Fig. 4b). This also leads to the movement of the magnetic vortex core in the spherical Fe-Co-rich phases, since the domain wall extends from the Heusler matrix into the Fe-Co-rich phases. However, even under high magnetic fields (Fig. 4f and i), the vortex-like structures remain stable. This strong interaction of the magnetic domains, leading to a connecting network of magnetic domain walls will promote a low permeability and high coercivity of the alloy.

The elongated Fe-Co-rich phases with a single magnetic domain (indicated by the green arrow in Fig. 4a) remain to have a single magnetic domain during the experiments. However, the domain wall contrast changes at 275 kA/m (Fig. 4e), indicating a spin reorientation in the domain. The spherical Fe-Co-rich phases having the vortex-like structure with subdomains (indicated by the blue arrows in Fig. 4a) remain unchanged, with an exception for the one indicated by the red arrow in Fig. 4a. This Fe-Co-rich phase remains a single magnetic domain structure (Fig. 4a-c) up to 124 kA/m, where it transforms into the vortex-like structure (Fig. 4d). The transition between the single magnetic domain and the vortex-like structure occurs when the magnetic domain wall in the Heusler phase crosses this phase. It then transforms back into the single domain when the magnetic field reaches 315 kA/m (Fig. 4f) and switches into the vortex-like structure at −126 kA/m (Fig. 4h) remaining in this state down to −214 kA/m (Fig. 4i). This indicates that a field dependent transition from single domain to vortex-like structure can occur in this two-phase alloy, which may further contribute to the bulk coercivity. Magnetic vortex structures have been predicted to be metastable [24] and yet, magnetic vortices in 3D $GdCo_2$ nanopillars are stable even when exposed to a magnetic field of up to 7 T [20]. The direction of the magnetic core in these magnetic vortices remains unchanged when altering the direction and strength of the magnetic field in this study. However, a direction reversal of the magnetic core and hence change in the swirl direction of vortices in the disordered A2 Fe-Cr-rich is observed under fields of 100–500 mT [10]. This is most likely determined by the relationship between the initial magnetization direction of the magnetic core and the external magnetic field direction.

To summarize, the microstructure, magnetic domain structure and its evolution under an external magnetic field of a soft magnetic dual-phase $Fe_{30}Co_{40}Ti_{10}Ge_{20}$ alloy were investigated using STEM-EDS, DPC-STEM, 4D-STEM and Lorentz TEM. Three types of Fe-Co-rich phases with different shapes were discerned in the Hesuler phase matrix: spherical, elongated and irregular. The magnetic domain type of the isolated Fe-Co-rich phases is shape-determined. Fe-Co-rich phases show a single magnetic domain structure when the aspect ratio $\delta > 1.6$ while developing into a vortex-like structure with subdomains with $1 < \delta < 1.6$. During *in situ* Lorentz TEM experiments, magnetic domain walls in the Heusler phase first start to move with the increase in the magnetic field, also promoting the movement of the magnetic vortex core in the spherical Fe-Co-rich phases due to a strong magnetic domain interaction. Most isolated Fe-Co-rich phases remain in their vortex-like domain state except that a magnetic domain structure switch between the single magnetic domain and the vortex-like structure was observed for a small spherical Fe-Co-rich phase. The evolution of stable vortex structures in spherical Fe-Co-rich phases and their interaction with magnetic domains and domain wall movement in the surrounding Heusler matrix is one important contribution to the bulk coercivity of the alloy.

Declaration of competing interests

The authors declare that they have no known competing financial interests or personal relationships that could have appeared to influence the work reported in this paper.

Acknowledgments

The authors gratefully acknowledge the support of Dr. Mingjian Wu and Prof. Erdmann Spiecker from the Institute of Micro- and Nanostructure Research (FAU) for providing access to the Spectra 200 microscope. We also greatly appreciate the assistance of Dr. Daniel Stroppa from DECTRIS for acquiring the 4D-STEM data. We thank Dr. Andras Kovacs (Ernst Ruska Center, Research Center Jülich) for providing the magnetic stray field data at the sample.

Supplementary materials

Supplementary material associated with this article can be found, in the online version, at doi:10.1016/j.scriptamat.2024.116097.

References

[1] L. Han, F. Maccari, I.R. Souza Filho, N.J. Peter, Y. Wei, B. Gault, O. Gutfleisch, Z. Li, D. Raabe, A mechanically strong and ductile soft magnet with extremely low coercivity, Nature 608 (2022) 310–316, https://doi.org/10.1038/s41586-022-04935-3.

[2] Z. Li, Z. Zhang, X. Liu, H. Li, E. Zhang, G. Bai, H. Xu, X. Liu, X. Zhang, Strength, plasticity and coercivity tradeoff in soft magnetic high-entropy alloys by multiple coherent interfaces, Acta. Mater. 254 (2023), https://doi.org/10.1016/j.actamat.2023.118970.

[3] C. Chen, H. Zhang, Y. Fan, W. Zhang, R. Wei, T. Wang, T. Zhang, F. Li, A novel ultrafine-grained high entropy alloy with excellent combination of mechanical and soft magnetic properties, J. Magn. Magn. Mater. 502 (2020), https://doi.org/10.1016/j.jmmm.2020.166513.

[4] P. Li, A. Wang, C.T. Liu, A ductile high entropy alloy with attractive magnetic properties, J. Alloys Compd. 694 (2017) 55–60, https://doi.org/10.1016/j.jallcom.2016.09.186.

[5] T. Borkar, B. Gwalani, D. Choudhuri, C.V. Mikler, C.J. Yannetta, X. Chen, R. V. Ramanujan, M.J. Styles, M.A. Gibson, R. Banerjee, A combinatorial assessment of $AlxCrCuFeNi_2$ ($0 < x < 1.5$) complex concentrated alloys: microstructure, microhardness, and magnetic properties, Acta. Mater. 116 (2016) 63–76, https://doi.org/10.1016/j.actamat.2016.06.025.

[6] K.B. Zhang, Z.Y. Fu, J.Y. Zhang, J. Shi, W.M. Wang, H. Wang, Y.C. Wang, Q. J. Zhang, Annealing on the structure and properties evolution of the CoCrFeNiCuAl high-entropy alloy, J. Alloys Compd. 502 (2010) 295–299, https://doi.org/10.1016/j.jallcom.2009.11.104.

[7] Y. Ikeda, B. Grabowski, F. Körmann, Ab initio phase stabilities and mechanical properties of multicomponent alloys: a comprehensive review for high entropy alloys and compositionally complex alloys, Mater. Charact. 147 (2019) 464–511, https://doi.org/10.1016/j.matchar.2018.06.019.

[8] D.B. Miracle, O.N. Senkov, A critical review of high entropy alloys and related concepts, Acta Mater. 122 (2017) 448–511, https://doi.org/10.1016/j.actamat.2016.08.081.

[9] L. Zhou, M.K. Miller, P. Lu, L. Ke, R. Skomski, H. Dillon, Q. Xing, A. Palasyuk, M. R. McCartney, D.J. Smith, S. Constantinides, R.W. McCallum, I.E. Anderson, V. Antropov, M.J. Kramer, Architecture and magnetism of alnico, Acta Mater. 74 (2014) 224–233, https://doi.org/10.1016/j.actamat.2014.04.044.

[10] Q. Lan, A. Kovács, J. Caron, H. Du, D. Song, S. Dasari, B. Gwalani, V. Chaudhary, R. V. Ramanujan, R. Banerjee, R.E. Dunin-Borkowski, Highly complex magnetic behavior resulting from hierarchical phase separation in AlCo(Cr)FeNi high-entropy alloys, iScience 25 (2022) 104047, https://doi.org/10.1016/j.isci.2022.104047.

[11] T. Radlinger, R. Winkler, P. Knoll, J. Zweck, H. Plank, F. Hofer, G. Kothleitner, A study on the correlation between micro and magnetic domain structure of $Cu_{52}Ni_{34}Fe_{14}$ spinodal alloys, J. Alloys Compd. 922 (2022), https://doi.org/10.1016/j.jallcom.2022.166214.

[12] A. Kovács, N.B. Venkataraman, V. Chaudhary, S. Dasari, T. Denneulin, R. V. Ramanujan, R. Banerjee, R.E. Dunin-Borkowski, Role of heterophase interfaces on local coercivity mechanisms in the magnetic $Al_{0.3}CoFeNi$ complex concentrated alloy, Acta Mater. 246 (2023), https://doi.org/10.1016/j.actamat.2023.118672.

[13] X. Zhang, L. Han, G. Dehm, C.H. Liebscher, Microstructure and physical properties of dual-phase soft magnetic Fe-Co-Ti-Ge alloys, J. Alloys Compd. 945 (2023) 169282, https://doi.org/10.1016/j.jallcom.2023.169282.

[14] J. Caron, EMPyRe - Electron Microscopy Reconstruction (2020), https://empyre.iffgit.fz-juelich.de/empyre/index.html#.

[15] K.X. Nguyen, X.S. Zhang, E. Turgut, M.C. Cao, J. Glaser, Z. Chen, M.J. Stolt, C. S. Chang, Y. Shao, S. Jin, G.D. Fuchs, D.A. Muller, Disentangling Magnetic and Grain Contrast in Polycrystalline FeGe Thin Films Using Four-Dimensional Lorentz Scanning Transmission Electron Microscopy, Phys. Rev. Appl. 10 (2022) 1, https://doi.org/10.1103/PhysRevApplied.17.034066.
[16] H. Oezelt, E. Kirk, P. Wohlhüter, E. Müller, L.J. Heyderman, A. Kovacs, T. Schrefl, Vortex motion in amorphous ferrimagnetic thin film elements, AIP Adv 7 (2017), https://doi.org/10.1063/1.4973295.
[17] A. Wachowiak, J. Wiebe, M. Bode, O. Pietzsch, M. Morgenstern, R. Wiesendanger, Direct Observation of Internal Spin Structure of Magnetic Vortex Cores, Science 298 (2002) 577–580, https://doi.org/10.1126/science.1075302.
[18] L.G. Korzunin, B.N. Filippov, F.A. Kassan-Ogly, On the vortex nature of the magnetization distribution in magnetic films, Phys. Met. Metall. 108 (2009) 538–542, https://doi.org/10.1134/S0031918X09120035.
[19] N.R. Cooper, Propagating magnetic vortex rings in ferromagnets, Phys. Rev. Lett. 82 (1999) 1554, https://doi.org/10.1103/PhysRevLett.82.1554.
[20] C. Donnelly, K.L. Metlov, V. Scagnoli, M. Guizar-Sicairos, M. Holler, N.S. Bingham, J. Raabe, L.J. Heyderman, N.R. Cooper, S. Gliga, Experimental observation of vortex rings in a bulk magnet, Nat. Phys. 17 (2021) 316–321, https://doi.org/10.1038/s41567-020-01057-3.
[21] N.A. Usov, M.S. Nesmeyanov, Multi-domain structures in spheroidal Co nanoparticles, Sci. Rep. (2020) 1–9, https://doi.org/10.1038/s41598-020-67173-5.
[22] M. Hanson, O. Kazakova, P. Blomqvist, R. Wäppling, B. Nilsson, Magnetic domain structures in submicron-size particles of epitaxial Fe (001) films: shape anisotropy and thickness dependence, Phys. Rev. B 66 (2002) 144419, https://doi.org/10.1103/PhysRevB.66.144419.
[23] S.P. Venkateswaran, N.T. Nuhfer, M. De Graef, Anti-phase boundaries and magnetic domain structures in Ni_2MnGa-type Heusler alloys, Acta Mater. 55 (2007) 2621–2636, https://doi.org/10.1016/j.actamat.2006.12.003.
[24] A. Bogdanov, A. Hubert, The Properties of Isolated Magnetic Vortices, Phys. Status Solidi 186 (1994) 527–543, https://doi.org/10.1002/pssb.2221860223.